Novel luminescent EuBTC@HA composite with dual sensing properties

Weronika Bodylska,*[a] Adam W. Augustyniak,[b] Dariusz C. Bieńko[c] and Marzena Fandzloch*[a]

[a] Institute of Low Temperature and Structure Research, Polish Academy of Sciences, Okólna 2, 50-422 Wrocław, Poland. E-mail: w.bodylska@intibs.pl, m.fandzloch@intibs.pl

[b] Faculty of Chemistry, University of Wrocław, F. Joliot-Curie 14, 50-383 Wrocław, Poland

[c] Faculty of Chemistry, Wroclaw University of Science and Technology, Wybrzeże Wyspiańskiego 27, 50-370 Wrocław, Poland

Table of contents

Figure S15. UV-Vis spectra of OFX solution at different concentrations before (a) and after detection using EuBTC@HA (b), along with a comparison of spectra for selected concentrations of $5.00 \cdot 10^{-3}$ M (c) and $3.13 \cdot 10^{-4}$ M (d).

Figure S16. Characterization of OFX and EuBTC@HA, before and after detection of OFX at concentrations of $3.13 \cdot 10^{-4}$ M and $5.00 \cdot 10^{-3}$ M using UV-Vis diffuse reflectance spectroscopy.

Figure S17. Overlay of the absorption spectrum of OFX (at a concentration of $5.00 \cdot 10^{-3}$ M) and the excitation spectrum of EuBTC@HA.

Table S2 Calculated HOMO and LUMO energies for H_3BTC and OFX.

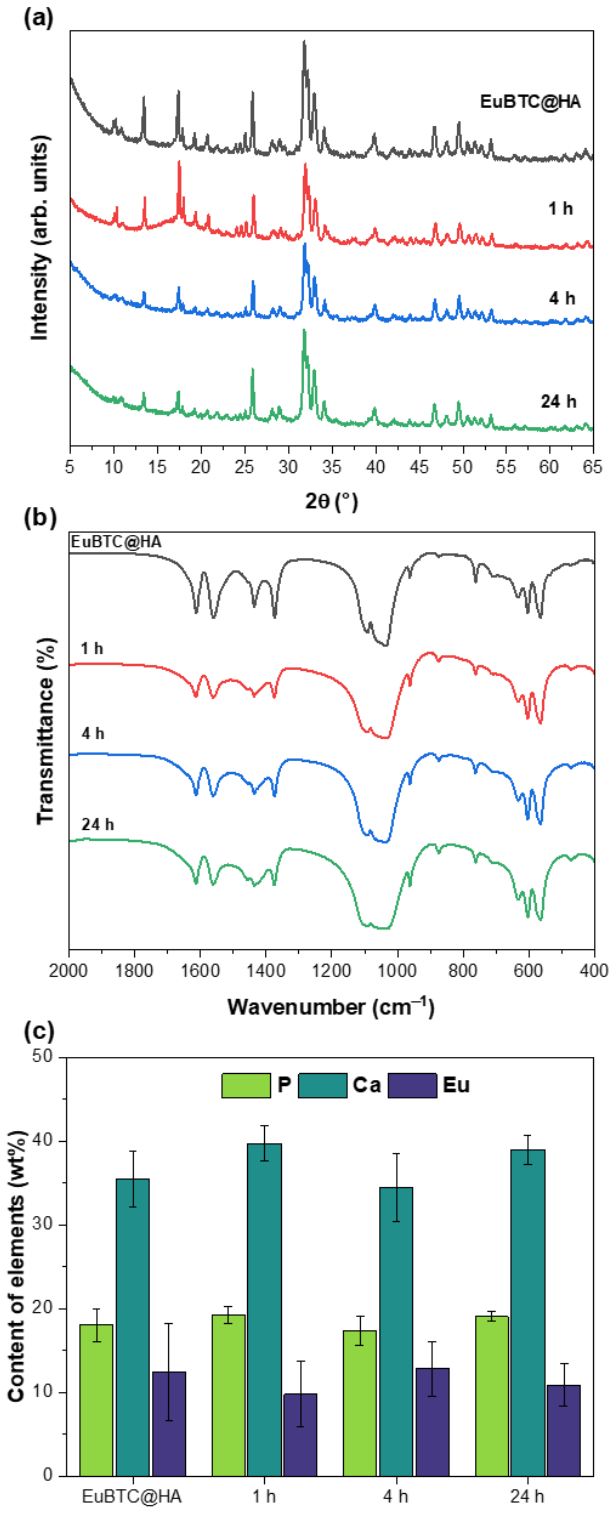

Figure S1. Stability of EuBTC@HA in water determined by PXRD (a), FT-IR spectroscopy (b), and analysis of composition monitored by EDS (c).

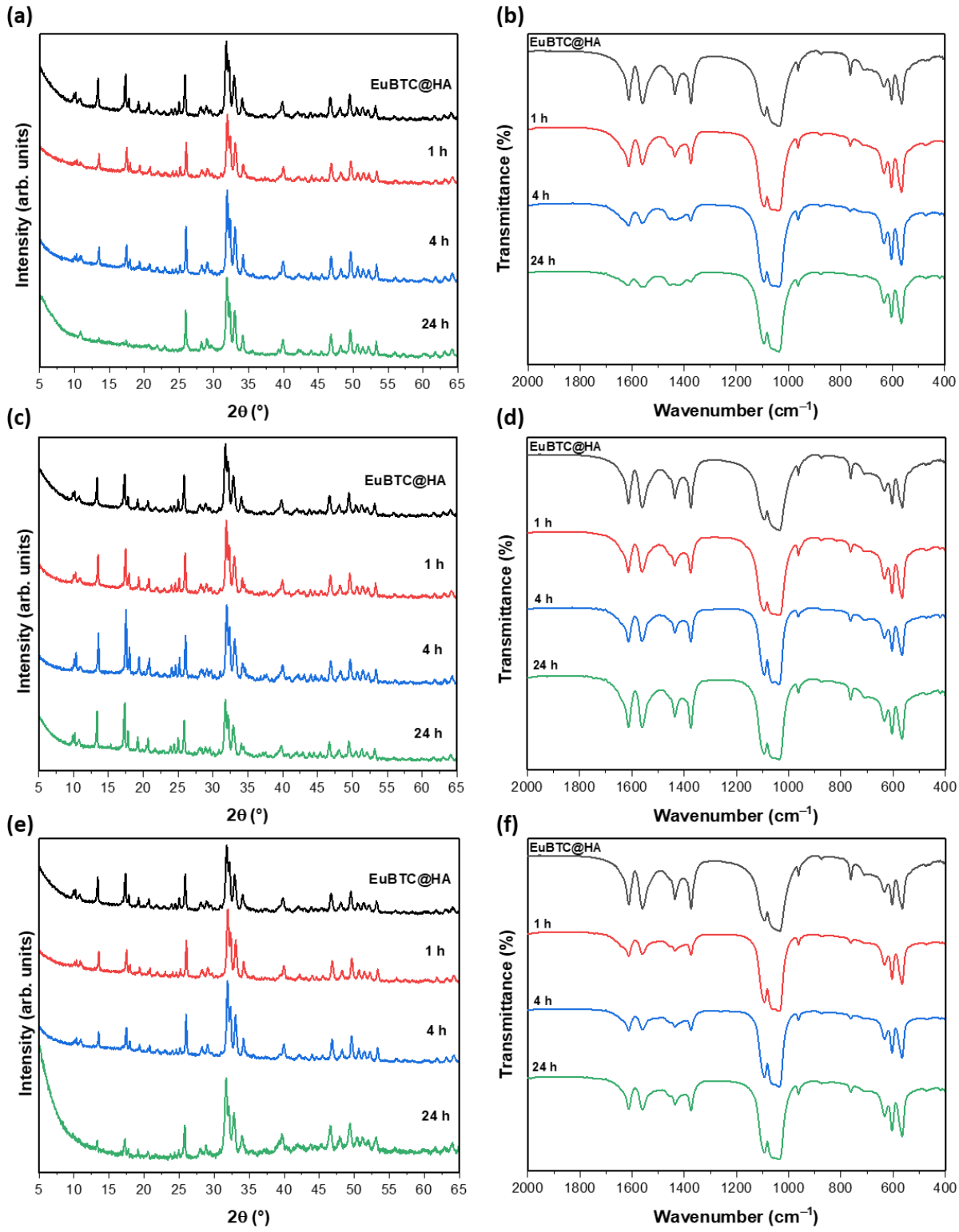

Figure S2. Stability of EuBTC@HA determined by PXRD (a,c,e) and FT-IR spectroscopy (b,d,f) in buffers of pH equal to 4.5 (a,b), 6.8 (c,d), and 8.8 (e,f), respectively.

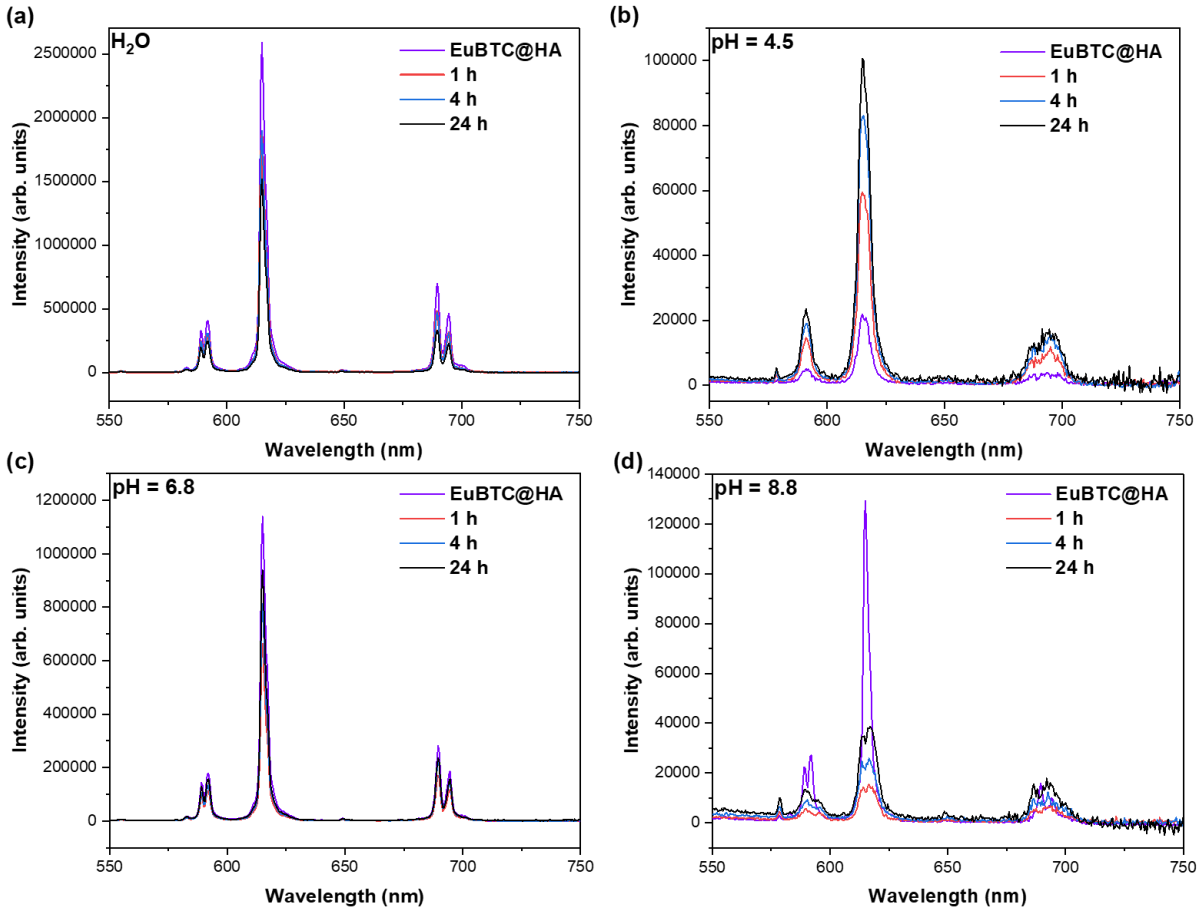

Figure S3. Fluorescence stability of EuBTC@HA over time in water (a), pH = 4.5 (b), pH = 6.8 (c), and pH = 8.8 (d).

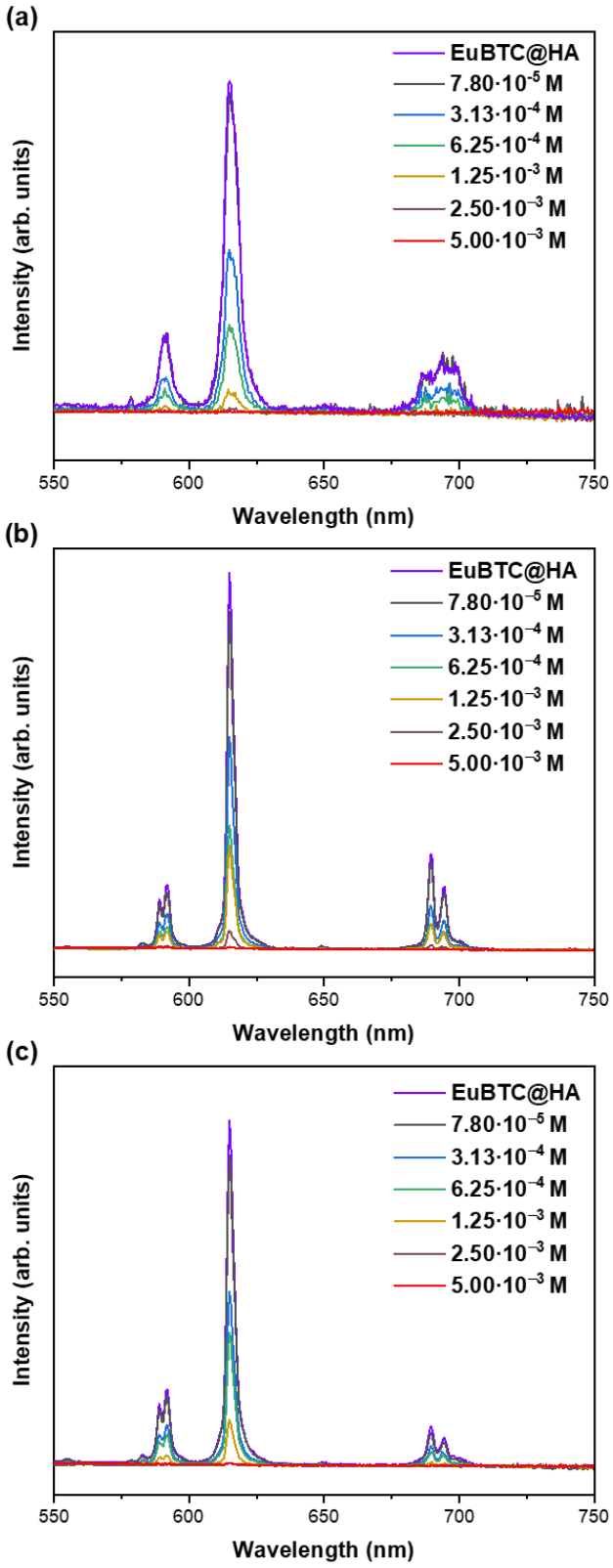

Figure S4. Emission spectra of EuBTC@HA for various concentrations of Fe^{3+} ions at pH 4.5 (a), 6.8 (b), and 8.8 (c).

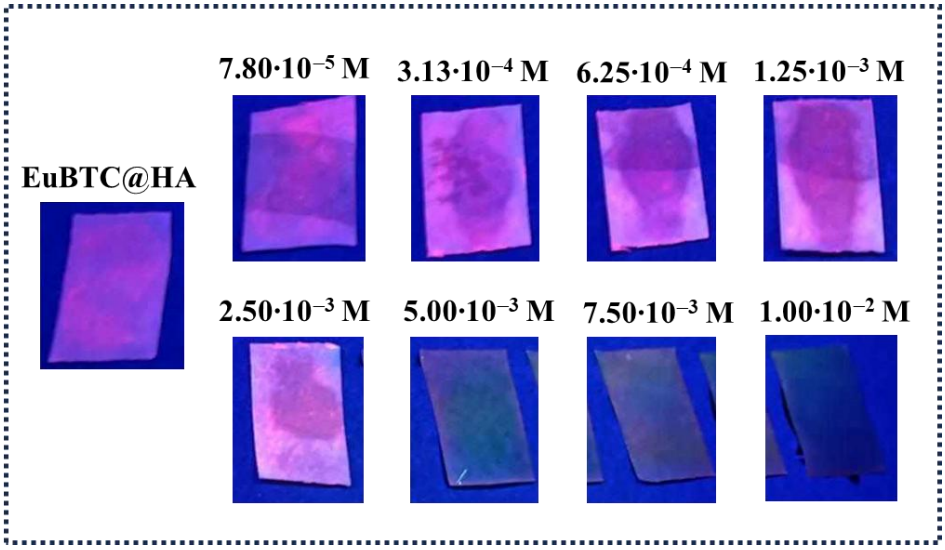

Figure S5. Photographs of the filter paper coated with EuBTC@HA used for the detection of Fe^{3+} ions in the concentration range of $7.80 \cdot 10^{-5}$ M to $1.00 \cdot 10^{-2}$ M under UV light ($\lambda = 254$ nm).

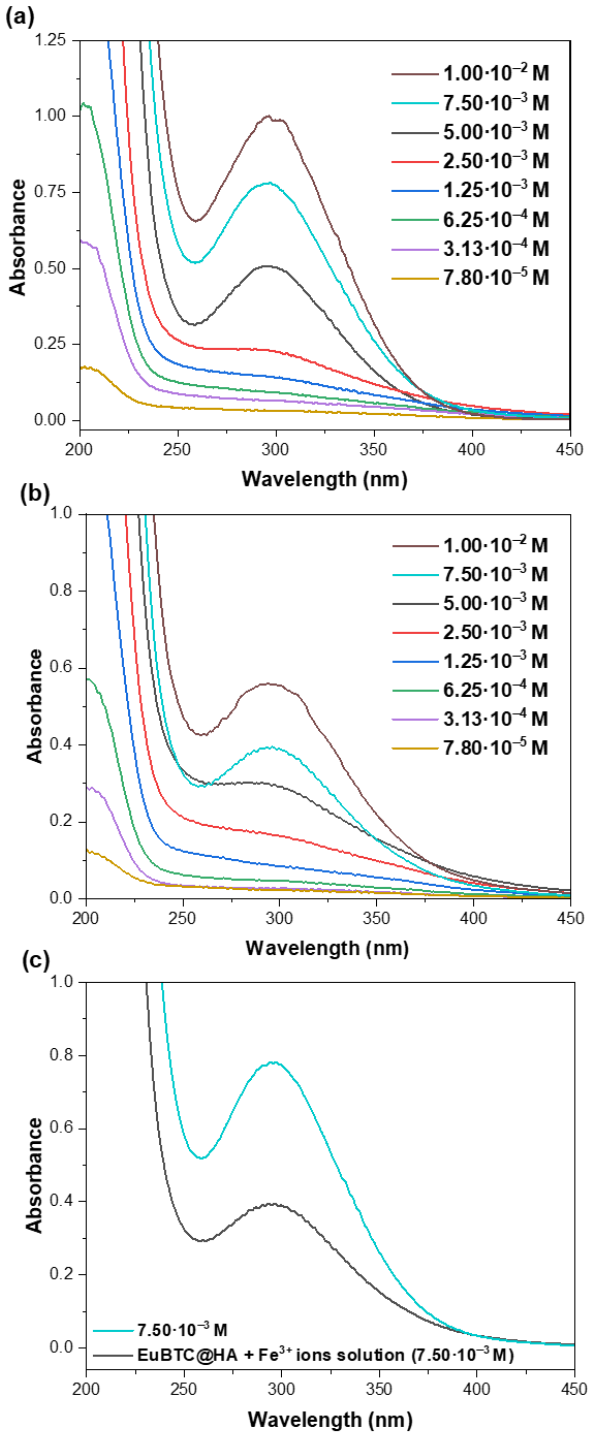

Figure S6. UV-Vis spectra of aqueous solution of iron(III) nitrate before (a) and after detection using EuBTC@HA (b), along with a comparison of the spectra for a selected concentration of $7.50 \cdot 10^{-3}$ M (c).

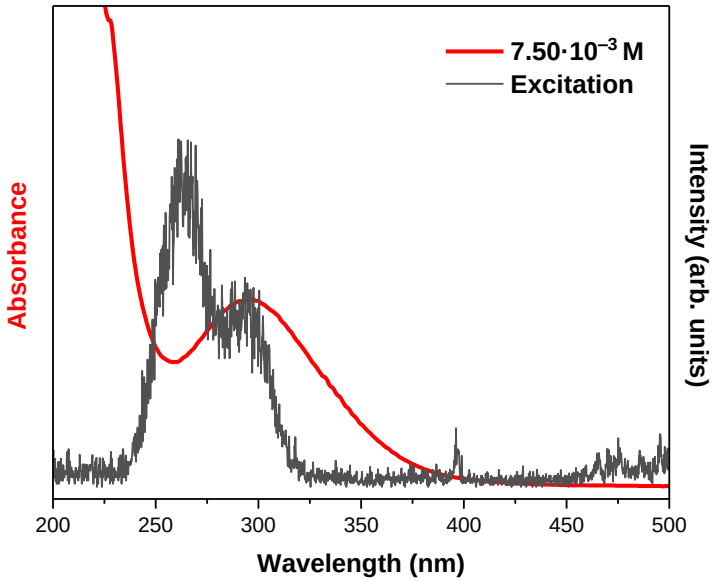

Figure S7. Overlay of the absorption spectrum of an aqueous solution of iron(III) nitrate (with a concentration of $7.50 \cdot 10^{-3}$ M) and the excitation spectrum of EuBTC@HA.

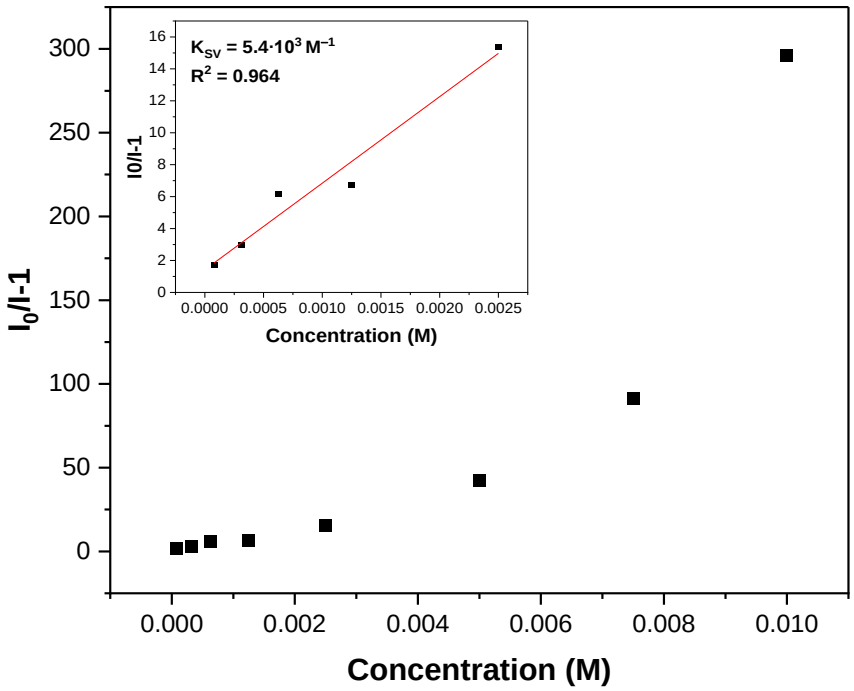

Figure S8. Stern–Volmer plot against the concentrations of iron(III) nitrate aqueous solutions with an inserted linear range.

Table S1. Average luminescence lifetimes of EuBTC@HA before and after detection of Fe^{3+} in the concentration range of $7.80 \cdot 10^{-5}$ M to $1.00 \cdot 10^{-2}$ M.

Concentration (M)	**Average lifetime (ms)**
EuBTC@HA	0.18
$7.80 \cdot 10^{-5}$	0.18
$3.13 \cdot 10^{-4}$	0.18
$6.25 \cdot 10^{-4}$	0.18
$1.25 \cdot 10^{-3}$	0.18
$2.50 \cdot 10^{-3}$	0.18
$5.00 \cdot 10^{-3}$	0.18
$7.50 \cdot 10^{-3}$	0.012
$1.00 \cdot 10^{-2}$	0.0075

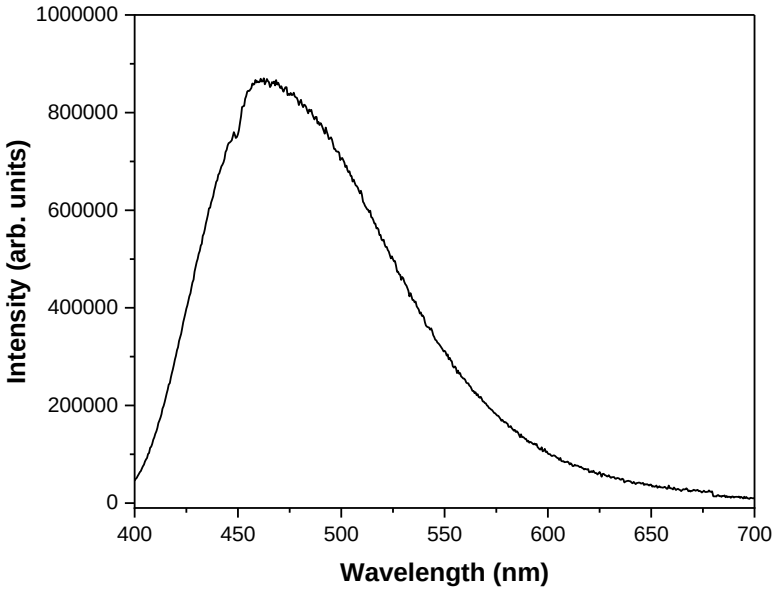

Figure S9. Emission spectrum of OFX at a concentration of $9.75 \cdot 10^{-6}$ M (λ_{exc} = 265 nm).

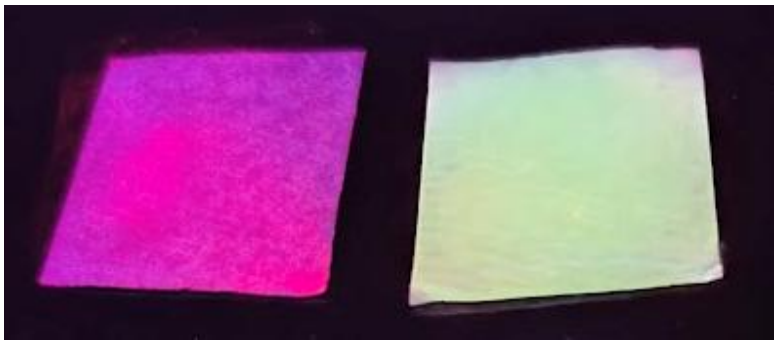

Figure S10. Photograph of the filter paper under UV light (λ = 254 nm) coated with EuBTC@HA (left) and after the addition of a few drops of OFX at a concentration of $2.43 \cdot 10^{-6}$ M (right).

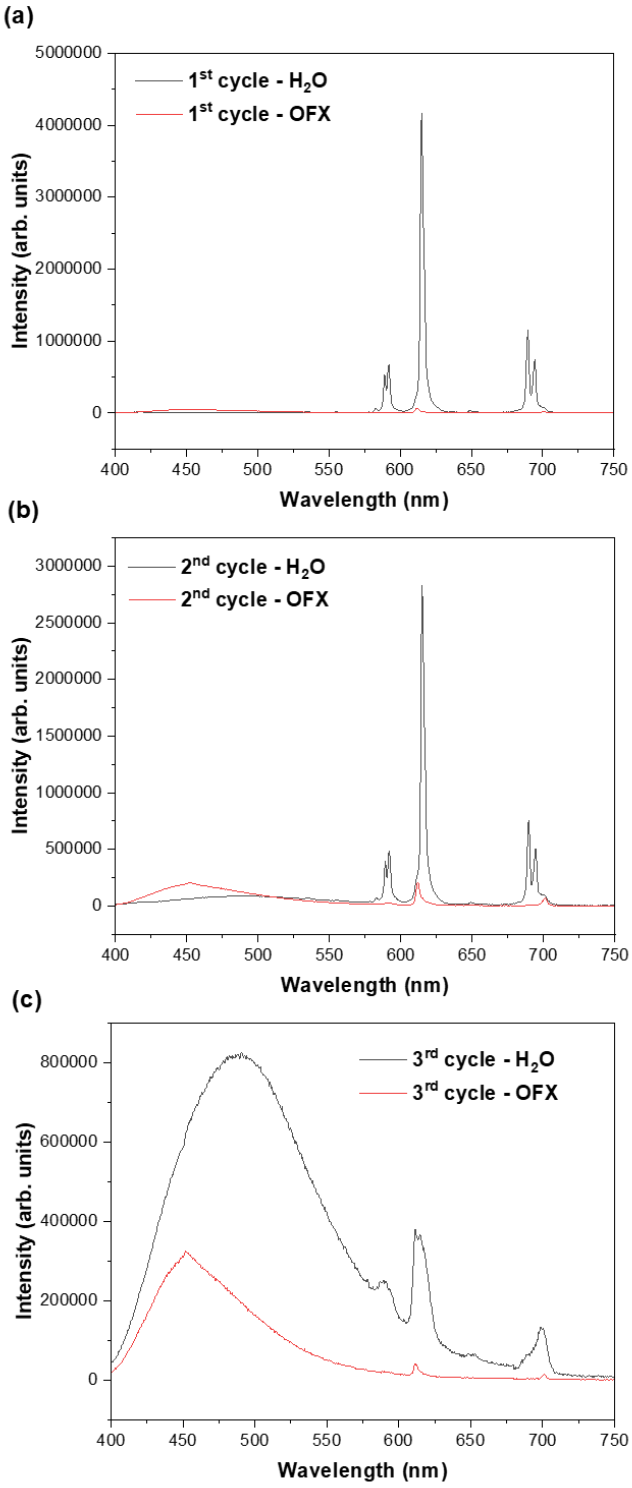

Figure S11. Emission spectra of EuBTC@HA after 1st (a), 2nd (b), and 3rd (c) cycle of OFX detection at a concentration of $5.00 \cdot 10^{-3}$ M.

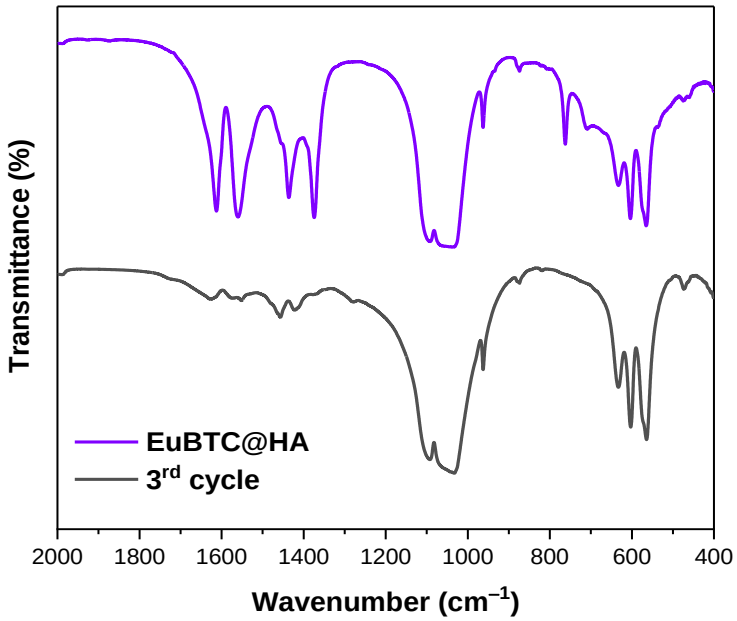

Figure S12. FT-IR spectra of EuBTC@HA before and after the 3rd cycle of OFX detection.

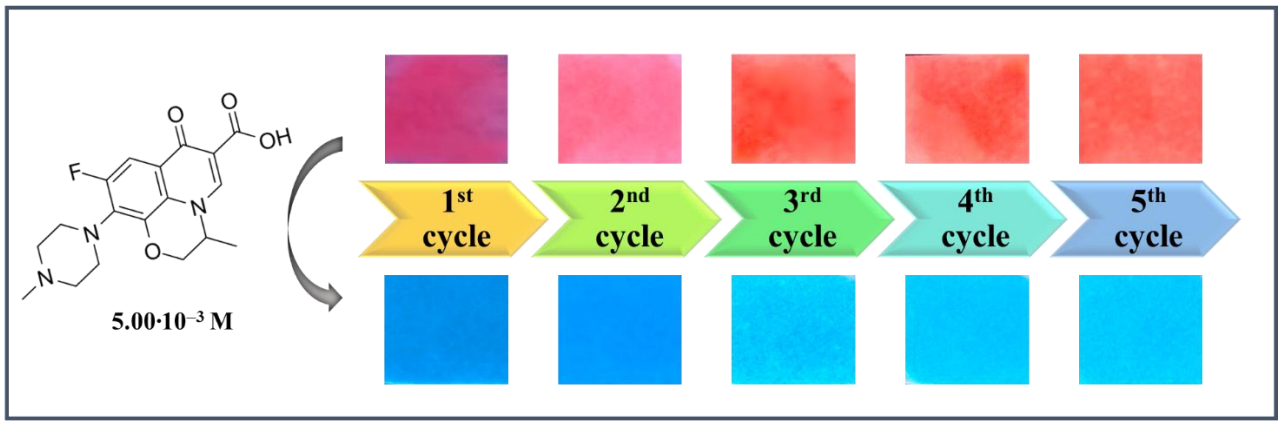

Figure S13. Photographs of the filter paper coated with EuBTC@HA used for the five cycles of OFX detection at a concentration of $5.00 \cdot 10^{-3}$ M under UV light ($\lambda = 254$ nm).

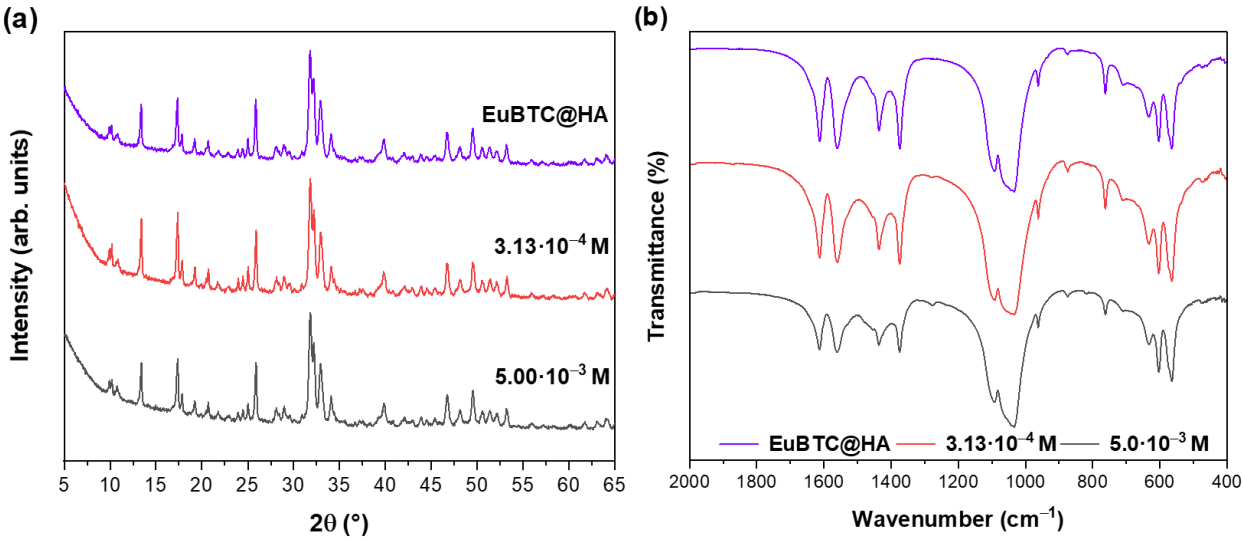

Figure S14. PXRD patterns (a) and FT-IR spectra (b) of EuBTC@HA before and after detection of OFX at concentrations of $3.13 \cdot 10^{-4}$ M and $5.00 \cdot 10^{-3}$ M.

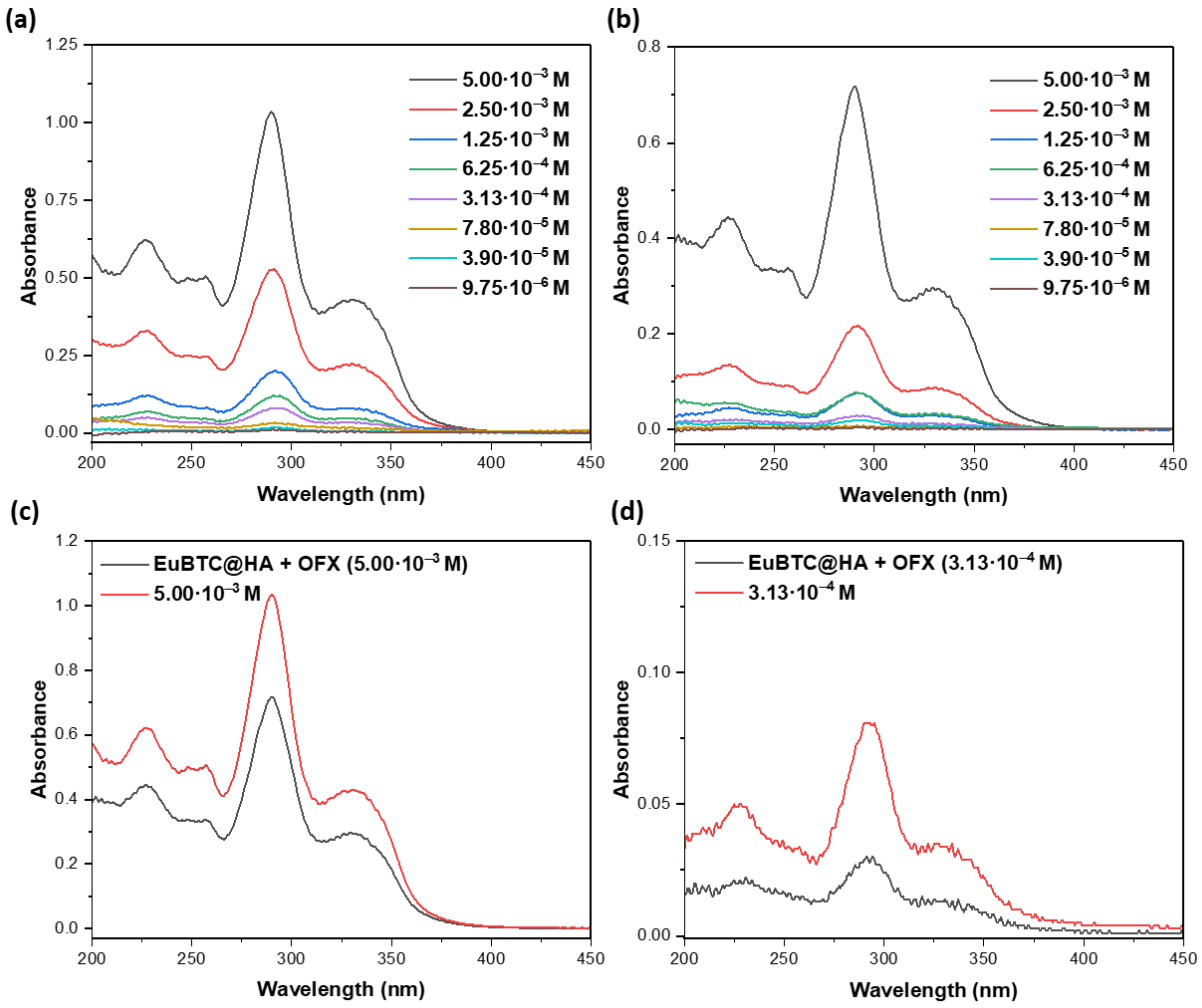

Figure S15. UV-Vis spectra of OFX solution at different concentrations before (a) and after detection using EuBTC@HA (b), along with a comparison of spectra for selected concentrations of $5.00 \cdot 10^{-3}$ M (c) and $3.13 \cdot 10^{-4}$ M (d).

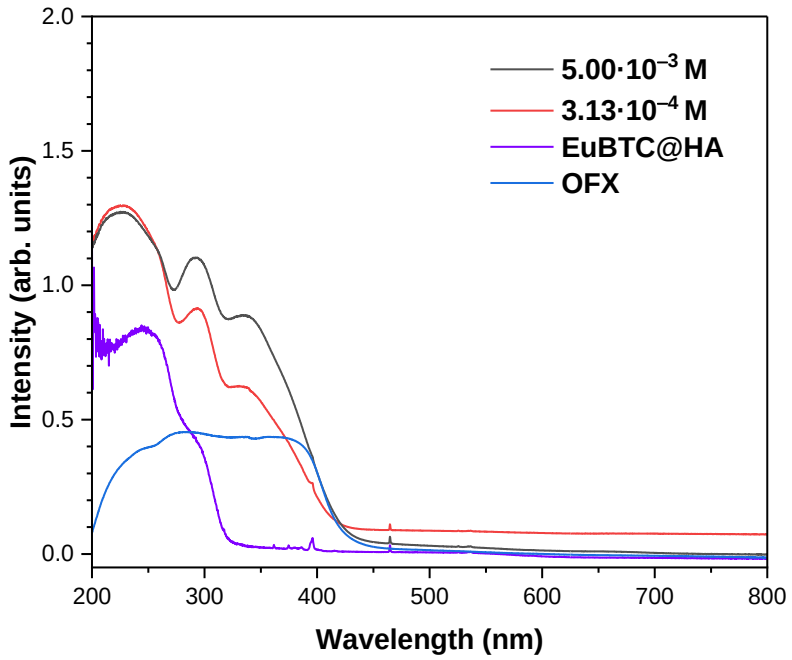

Figure S16. Characterization of OFX and EuBTC@HA, before and after detection of OFX at concentrations of $3.13 \cdot 10^{-4}$ M and $5.00 \cdot 10^{-3}$ M using UV-Vis diffuse reflectance spectroscopy.

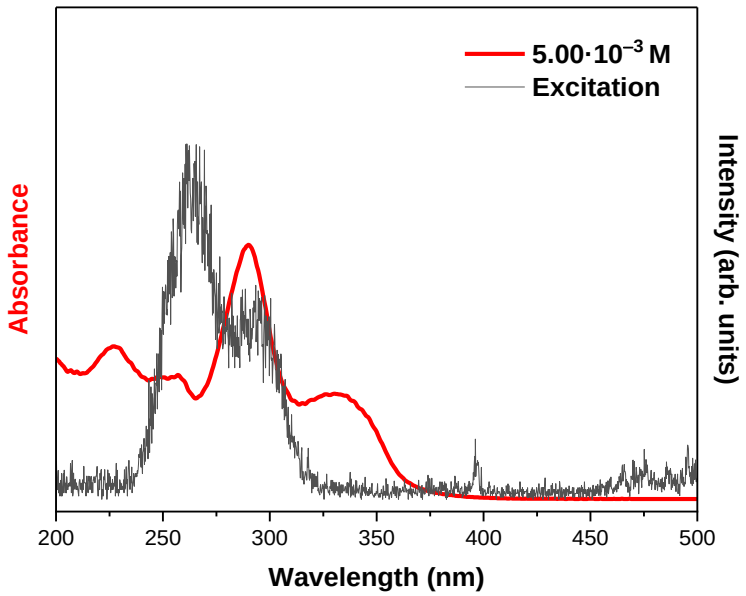

Figure S17. Overlay of the absorption spectrum of OFX (at a concentration of $5.00 \cdot 10^{-3}$ M) and the excitation spectrum of EuBTC@HA.

Table S2 Calculated HOMO and LUMO energies for H_3BTC and OFX.

	E_{HOMO} (eV)	E_{LUMO} (eV)	$\Delta E(E_{LUMO} - E_{HOMO})$ (eV)
H_3BTC	-8.0501	-2.361	5.689
OFX	-6.151	-1.948	4.203